Journal of Power Sources 253 (2014) 187–192

Contents lists available at ScienceDirect

Journal of Power Sources

journal homepage: www.elsevier.com/locate/jpowsour

Effect of $Ce_{0.8}Sm_{0.2}O_{1.9}$ interlayer on the electrochemical performance of $La_{0.75}Sr_{0.25}Cr_{0.5}Mn_{0.5}O_{3-\delta}$–$Ce_{0.8}Sm_{0.2}O_{1.9}$ composite anodes for intermediate-temperature solid oxide fuel cells

Shoucheng He, Han Chen, Ruifeng Li, Lin Ge, Lucun Guo*

College of Materials Science and Engineering, Nanjing University of Technology, No. 5 Xinmofan Road, Nanjing, Jiangsu 210009, PR China

HIGHLIGHTS

- Alternative anodes of LSCM–SDC were prepared and investigated for IT-SOFCs.
- Compositions of LSCM–SDC composite anodes were optimized.
- SDC interlayer was effective for improving the performance of LSCM–SDC anodes.
- Outstanding intermediate-temperature electrochemical performance was achieved.

ARTICLE INFO

Article history:
Received 10 September 2013
Received in revised form
16 December 2013
Accepted 16 December 2013
Available online 21 December 2013

Keywords:
Solid oxide fuel cell
Composite anode
Interlayer
Electrochemical performance

ABSTRACT

Composite anodes of $La_{0.75}Sr_{0.25}Cr_{0.5}Mn_{0.5}O_{3-\delta}$–$Ce_{0.8}Sm_{0.2}O_{1.9}$ (LSCM–SDC) were prepared and investigated as anode materials for intermediate-temperature solid oxide fuel cells (IT-SOFCs) with YSZ electrolyte. Results showed that the addition of SDC significantly enhanced the electrochemical performance of LSCM anode. The anode containing 40 wt.% SDC demonstrated optimal performance. The polarization resistance and anodic overpotential (at a current density of 0.05 A cm^{-2}) of this anode were 0.95 Ω cm^2 and 0.12 V in H_2 at 800 °C, respectively, whereas those of pure LSCM anode were 3.66 Ω cm^2 and 0.38 V, respectively. The electrochemical performance of the LSCM–40SDC composite anode was further improved when a thin SDC interlayer was coated between the anode and YSZ electrolyte. The resulting polarization resistance and anodic overpotential with the SDC interlayer were 0.30 Ω cm^2 and 0.035 V in H_2 at 800 °C, demonstrating a reduction by factors of 3.2 and 3.4, respectively. The impedance data displayed that the coated SDC interlayer mainly affected the low frequency electrode process, indicating that the SDC interlayer played an important role in the promotion of the dissociation and diffusion processes of H_2 oxidation reaction.

1. Introduction

Solid oxide fuel cells (SOFCs) are highly promising energy conversion devices because of their high conversion efficiency, low pollutant output, and great fuel flexibility [1]. At present, the development of SOFCs is mainly based on yttria-stabilized zirconia (YSZ) electrolyte due to its high oxide ion conductivity, good thermal and chemical stability and high mechanical strength [2]. The most common anode material for YSZ-based SOFCs is Ni/YSZ cermet, where Ni displays excellent catalytic activity to fuel oxidation and high electronic conductivity, and YSZ provides ionic conductivity and structural support [3]. However, this material also exhibits some disadvantages, such as agglomeration and coarsening of the Ni phase after long-term operation, carbon deposition in hydrocarbon fuel applications, and low sulfur tolerance resulting from NiS formation [4–6].

To overcome the disadvantages of Ni/YSZ anode, several Ni-free oxides such as ceria-based, $LaCrO_3$-based, and $SrTiO_3$-based oxides have attracted significant attention as alternative anodes [7–9]. Among them, $LaCrO_3$-based oxides have been extensively investigated as interconnect materials for SOFCs because of their high redox stability even at high temperatures (e.g., 1000 °C) [1]. Recently, Sfeir et al. [10,11] studied the catalytic activity and thermodynamic stability of substituted lanthanum chromites. They found that the A-site substitution of Ca and Sr and the B-site substitution of Mn and Fe improve the catalytic activity. Meanwhile, Sr and Mn substitution maintains the stability of the perovskite, whereas the others destabilize the

* Corresponding author. Tel.: +86 25 83587261; fax: +86 25 83306152.
E-mail address: lc-guo@163.com (L. Guo).

0378-7753/$ – see front matter © 2013 Elsevier B.V. All rights reserved.
http://dx.doi.org/10.1016/j.jpowsour.2013.12.071

system. The performance of the most commonly studied material, $La_{0.75}Sr_{0.25}Cr_{0.5}Mn_{0.5}O_{3-\delta}$ (LSCM), is comparable with that of Ni/YSZ in both H_2 and CH_4 [2,12].

Creation of composite anodes is a good way to enhance the catalytic activity and reduce the polarization resistance of anodes. Moreover, composite anodes have thermal expansion coefficients (TECs) that match those of other cell components. The performance of LSCM anode can be improved by adding YSZ electrolyte to produce a composite anode [13]. The optimum performance was achieved with 50–60 wt.% LSCM contents sintered at 1200 °C. In addition, composites such as LSCM–$Gd_{0.1}Ce_{0.9}O_{2-\delta}$ (GDC) [14,15] and LSCM–$La_{0.2}Ce_{0.8}O_{2-\delta}$ (LDC) [16] are also well-known examples. It is widely accepted that composite anodes can expand the reaction zone beyond the three-phase boundary (TPB) and improve the adhesion between the anode and electrolyte, resulting in enhanced anode performance [17–19]. Murray et al. [20] reported that introducing a ceria-based interlayer between the anode and electrolyte can enhance the anode performance. A $(Y_2O_3)_{0.15}(CeO_2)_{0.85}$ (YDC) interlayer deposited on YSZ electrolyte can reduce the polarization resistance of Ni/YSZ anode by a factor of ~6.

Previous studies have reported that Sm-doped ceria (SDC) has the highest ionic conductivity among the singly doped ceria [21–23]. In the present study, LSCM–SDC composite anodes were fabricated and investigated as anode materials for intermediate-temperature SOFCs with YSZ electrolyte. The optimal SDC content was identified to exhibit the best performance. Furthermore, we evaluated the effect of the SDC interlayer on the electrochemical performance of the prepared LSCM–SDC composite anode.

2. Experiment

2.1. Powder synthesis

LSCM and SDC powders were synthesized using a conventional solid state reaction method. Stoichiometric amounts of La_2O_3 (99.5%), $SrCO_3$ (99.0%), Cr_2O_3 (99.9%), $MnCO_3$ (99.0%), CeO_2 (99.99%), and Sm_2O_3 (99.99%) were mixed in distilled water and then milled for 8 h. After drying and grinding, the powders were calcined at 1400 °C for 24 h and at 1200 °C for 2 h, respectively. The LSCM–*x*SDC (x = 10–50 wt.%) composite anodes were prepared by mixing and milling as-synthesized LSCM and SDC powders with appropriate weight ratio.

2.2. Sample preparation

YSZ was selected as the electrolyte and prepared by the solid state reaction method. Y_2O_3 (99.99%) and ZrO_2 (99.9%) were used as starting materials. After milling, granulation and dry pressing processes, the pellets were sintered at 1600 °C for 4 h to yield the electrolyte with 16 mm in diameter and 1.2 mm in thickness.

A mixture of ethyl cellulose and terpinol was used to prepare the SDC slurry and LSCM–*x*SDC composite anode slurry. The composite anode slurry was printed on both sides of the YSZ electrolyte with a surface area of 0.5 cm^2 by screen printing method and then calcined at 1300 °C for 2 h in air. The SDC interlayer between the composite anode and electrolyte was prepared in the same manner. The YSZ pellet was sequentially coated with the SDC slurry and composite anode slurry by screen printing method and then sintered together at 1300 °C for 2 h in air. Ag paste as the current collector and the reference electrode was painted onto the electrode and electrolyte surfaces. The reference electrode was placed approximately 3 mm away from the working electrode. The painted Ag was heated at 750 °C for 0.5 h in air.

LSCM–*x*SDC powders were pressed to form a bar with dimensions of 3 mm × 5 mm × 50 mm and then sintered at 1300 °C for 2 h to investigate the thermal expansion and electrical conductivity of the composite anodes.

2.3. Characterization

The crystal structure of the synthesized powders was characterized by X-ray diffraction (XRD, ARL X'TRA diffractometer) with Cu Kα radiation (λ = 0.15418 nm). The diffractometer was operated at 40 kV and 35 mA in the 2θ range of 20°–80°. The microstructure of the cross-section was evaluated by scanning electron microscopy (SEM, Model JSM-5900) at an accelerating voltage of 15 kV. The working distance was 10 mm and secondary electron signal was used for imaging.

The thermal expansion of the composite anodes was analyzed by a dilatometer (RPZ-01, Luoyang, China) in air from 25 °C to 800 °C at a heating rate of 5 °C min^{-1}. The electrical conductivity of the anodes was measured by a conventional DC four-probe method from 200 °C to 800 °C in air.

The electrochemical performance of the anodes was investigated by an electrochemical workstation (PARSTAT 2273) from 650 °C to 800 °C in wet H_2. The electrochemical impedance spectra (EIS) were measured by a symmetric cell in the frequency range of 0.01 Hz to 100 kHz with an AC amplitude of 10 mV. The impedance spectra were analyzed by the equivalent circuit of ZSimpWin software. The anodic polarization was tested by a three-electrode system at 800 °C. The electrochemical measurements were conducted in wet H_2 at a flow rate of 30 mL min^{-1}, which was controlled by a mass flow meter (Sevenstar D07-19B).

3. Results and discussion

3.1. Crystal structure and chemical compatibility

The XRD patterns of the SDC and LSCM powders are shown in Fig. 1. The SDC powder exhibits corresponding cubic fluorite structure phase with a slight Sm_2O_3 peak after calcining at 1200 °C for 2 h. The pattern of LSCM in Fig. 1 is identical to the LSCM reported by Tao et al. [2], indicating the appearance of perovskite structure phase. Although several slight peaks are observed (La_2O_3 and $Mn_{1.5}Cr_{1.5}O_4$), their influence on the performance of anodes is negligible because of their minimal content.

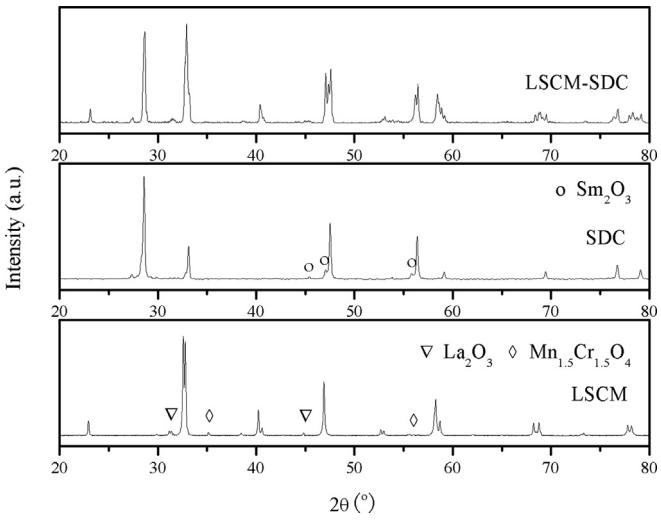

Fig. 1. XRD patterns of the LSCM, SDC and composite LSCM–SDC powders.

The LSCM powder was mixed with the SDC powder at a 1:1 weight ratio and then calcined at 1300 °C for 2 h to investigate the chemical compatibility of LSCM with SDC. The XRD pattern of the composite LSCM–SDC powder is shown in Fig. 1. No phase change and no secondary phase appear after heat treatment, indicating that LSCM has good chemical compatibility with SDC.

3.2. Thermal expansion

The TECs of SOFCs components should match with each other to avoid causing internal stress and cracking, which strongly affect the stability and lifetime of SOFCs. The thermal expansion curves of the LSCM–*x*SDC anodes calcined at 1300 °C from 25 °C to 800 °C in air are shown in Fig. 2. The thermal expansion of all composite anodes exhibits a linear increase with the elevated temperature. The average TECs were calculated from the thermal expansion data according to the following equation:

$$\alpha = \frac{dL}{L_0} \times \frac{1}{T_2 - T_1} \quad (1)$$

where α is the average TEC in the temperature range of T_1 to T_2, L_0 is the initial length of the sample and dL is the change in the length of the sample in the temperature range of T_1 to T_2.

The average TECs calculated from the thermal expansion data are listed in Fig. 2. The TECs of the LSCM–*x*SDC anodes range from 11.79 × 10^{-6} K^{-1} to 11.59 × 10^{-6} K^{-1}, whereas that of LSCM is 11.63 × 10^{-6} K^{-1}, indicating that the effect of SDC on the TECs of the composite anodes is negligible. Jiang et al. [13] reported that the TEC of LSCM is 11.4 × 10^{-6} K^{-1} after sintering at 1200 °C for 2 h. The TEC value strongly depends on the porosity of sample, while the porosity of anodes should be more than 30% to obtain effective reaction area and gas channel [24]. High porosity complicates the determination of changes in TEC. Moreover, Zheng et al. [23] reported that the TEC of SDC is 12.62 × 10^{-6} K^{-1}, which is close to that of LSCM. This result indicates that the TECs of all composite anodes are not significantly different from that of pure LSCM.

3.3. Electrical conductivity

A previous study reported that the electrical conductivity and activation energy (E_a) of LSCM are 38.6 S cm^{-1} at 900 °C and 0.21 eV between 92 °C and 900 °C in air [2], respectively. The Arrhenius plots of the conductivity of the LSCM–*x*SDC composite anodes in air are shown in Fig. 3. A linear relationship exists between $\ln(\sigma T)$ and $1000/T^{-1}$ for all anodes, and the E_a values calculated from the slope of the plots range from 0.199 eV to 0.213 eV, indicating that the electrical conductivity of all anodes is generally attributed to small polaron hopping mechanism. The conductivity of LSCM and LSCM–*x*SDC (x = 10–50 wt.%) at 800 °C are 32.1, 15.4, 11.1, 3.69, 2.08, and 0.35 S cm^{-1}, respectively, demonstrating that the decreased conductivity of the anodes with increasing SDC content.

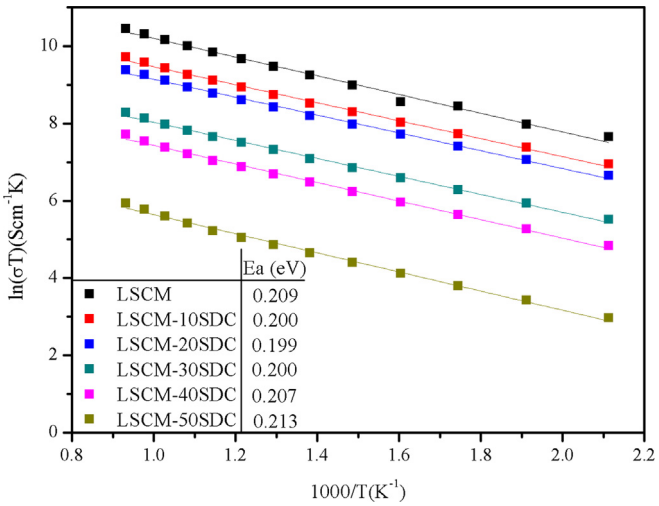

Fig. 3. Arrhenius plots of the conductivity of the LSCM–*x*SDC anodes.

3.4. Electrochemical performance

The EIS of the LSCM–*x*SDC anodes at 800 °C in wet H_2 at open circuit potential are shown in Fig. 4. The EIS were fitted by the equivalent circuit of $R_{ohm}(Q_1R_1)(Q_2R_2)$. R_{ohm} is the total ohmic resistance of the cell, including the electrolyte, electrodes, current collectors, and lead wires, corresponding to the intercept on the real axis at high frequency. R_1 and R_2 are the electrode polarization resistances at high and low frequencies, respectively. The anode polarization resistance R_P is the sum of R_1 and R_2. The R_{ohm} in the

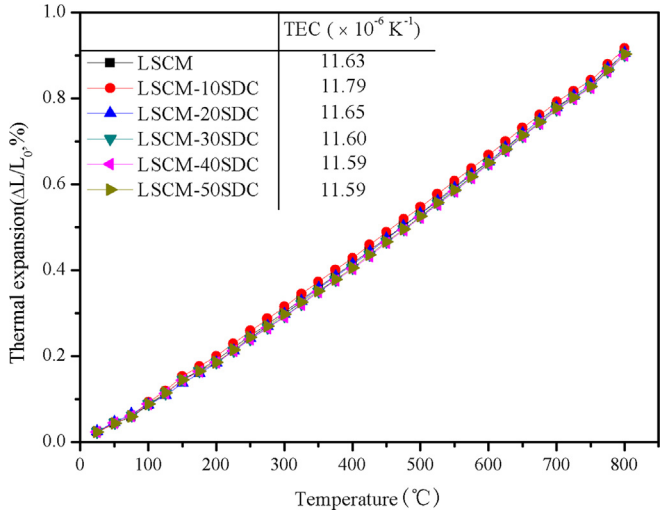

Fig. 2. Thermal expansion curves of LSCM–*x*SDC from 25 °C to 800 °C in air.

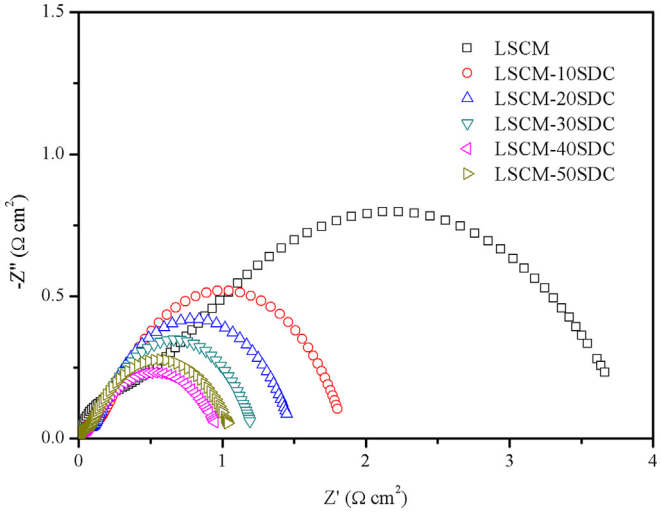

Fig. 4. Impedance spectra of the LSCM–*x*SDC anodes at 800 °C in H_2.

EIS was subtracted to directly compare the R_P of different anodes. It can be seen the addition of SDC significantly reduces the R_P of LSCM anode. The R_P of the LSCM–*x*SDC composite anodes initially decreases and then slightly increases with increasing SDC content, reaching a minimum at 40 wt.% SDC.

The R_P values of anodes calculated from the EIS at 650–800 °C are provided in Table 1. The R_P of LSCM anode at various temperatures is markedly reduced by adding SDC. The lowest R_P value is 0.95 Ω cm^2 at 800 °C when the SDC content of the composite anode is 40 wt.%, whereas the R_P of pure LSCM anode is 3.66 Ω cm^2. Deleebeeck et al. [25] reported that the R_P of $La_{0.8}Sr_{0.2}Cr_{0.5}Mn_{0.5}O_{3-\delta}$ anode decreases from 8.6 Ω cm^2 to 0.74 Ω cm^2 at 800 °C in H_2 when the anode is mixed with 50 wt.% GDC. Ruiz-Morales et al. [17] reported that the R_P of LSCM under humidified 5% H_2 exhibits a significant improvement for the 50:50 composite of YSZ and GDC. The R_P is reduced from 1.8 Ω cm^2 to 0.8 Ω cm^2 at 950 °C.

The lower R_P of the composite anodes compared with pure LSCM anode is attributed to the increase in ionic conductivity and catalytic activity towards H_2 oxidation that occurs by adding SDC [26]. Furthermore, the addition of SDC may improve the adhesion between YSZ electrolyte and anode [25]. However, LSCM–50SDC exhibits slightly higher R_P than LSCM–40SDC because of the low electrical conductivity of SDC, resulting in a slow charge transfer process [16]. Considering the low electrical conductivity of LSCM–50SDC and the results in Fig. 3, we selected LSCM–40SDC as the optimal anode.

Fig. 5 shows the polarization overpotential of the LSCM–*x*SDC anodes at 800 °C in wet H_2. The LSCM–40SDC anode exhibits the lowest overpotential, corresponding to the result of EIS in Fig. 4. The anodic overpotential values of the LSCM–*x*SDC anodes at a current density of 0.05 A cm^{-2} at 800 °C are approximately 0.22, 0.18, 0.17, 0.12, and 0.13 V, respectively, which are considerably lower than that of pure LSCM (0.38 V). Babaei et al. [27] reported that the polarization performance of $La_{0.7}Ca_{0.3}Cr_{0.5}Mn_{0.5}O_{2.6}$–GDC strongly depends on sintering temperature. The overpotential value for the anode sintered at 1200 °C is approximately 0.10 V at a current density of 0.05 A cm^{-2} and a temperature of 800 °C.

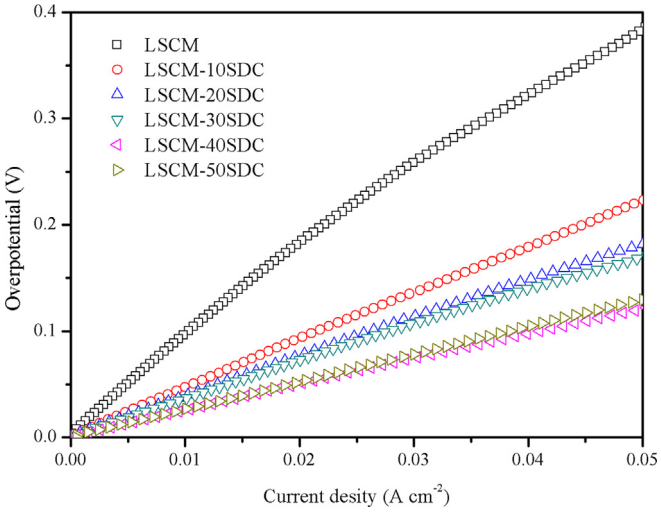

Fig. 5. Anodic overpotential of the LSCM–*x*SDC anodes at 800 °C in H_2.

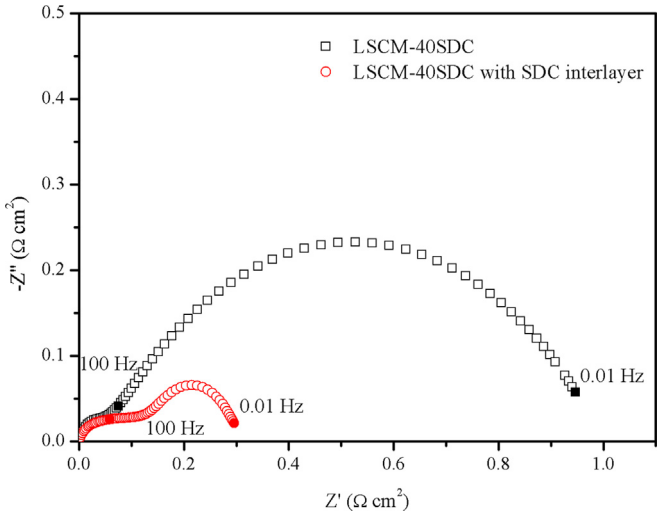

Fig. 6. Impedance spectra of the LSCM–40SDC anodes without and with the SDC interlayer at 800 °C in H_2.

3.5. Effect of SDC interlayer on electrochemical performance

The EIS of the LSCM–40SDC anodes without and with the SDC interlayer are shown in Fig. 6. The impedance data were obtained at 800 °C in wet H_2 at open circuit potential. It is observed that the R_P of the LSCM–40SDC anode is significantly reduced by a factor of 3.2 with the SDC interlayer.

The EIS in Fig. 6 consist of two arcs, i.e. a small high frequency arc and a large low frequency arc. The polarization resistance of the high frequency arc (R_1) is related to charge transfer process, whereas that of the low frequency arc (R_2) is related to dissociation and diffusion processes [28].

The R_1, R_2 and R_P of the LSCM–40SDC anodes without and with the SDC interlayer obtained from the fits to the EIS are listed in Table 2.

Table 2
Polarization resistance of the LSCM–40SDC anodes without and with the SDC interlayer obtained from the fits to the EIS.

T (°C)	LSCM–40SDC			LSCM–40SDC with SDC interlayer		
	R_1 (Ω cm^2)	R_2 (Ω cm^2)	R_P (Ω cm^2)	R_1 (Ω cm^2)	R_2 (Ω cm^2)	R_P (Ω cm^2)
700	0.16	2.65	2.81	0.14	0.85	0.99
750	0.09	1.52	1.61	0.08	0.40	0.48
800	0.08	0.87	0.95	0.06	0.24	0.30

Table 1
Polarization resistance of the LSCM–SDC composite anodes at 650–800 °C in H_2.

T (°C)	Polarization resistance (Ω cm^2)					
	LSCM	LSCM–10SDC	LSCM–20SDC	LSCM–30SDC	LSCM–40SDC	LSCM–50SDC
650	11.7	5.78	5.64	5.38	5.11	5.24
700	8.76	3.94	3.57	3.09	2.81	2.90
750	5.60	2.52	2.17	1.84	1.61	1.69
800	3.66	1.80	1.45	1.19	0.95	1.04

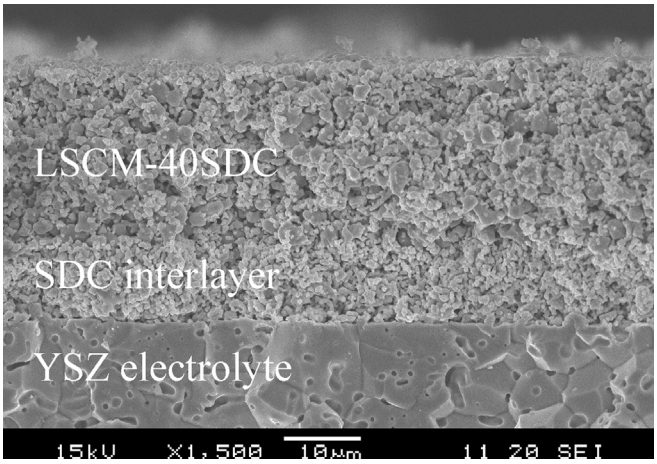

Fig. 7. SEM image of the cross-section of the LSCM–40SDC anode with the SDC interlayer.

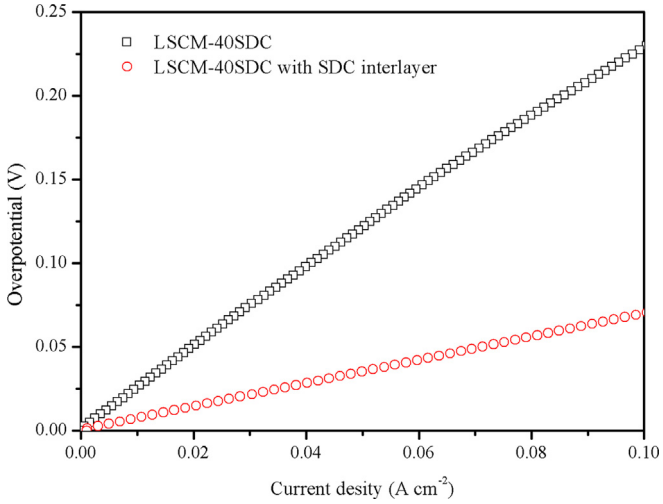

Fig. 8. Anodic overpotential of the LSCM–40SDC anodes without and with the SDC interlayer at 800 °C in H_2.

Table 2. R_2 is considerably higher than R_1 at various temperatures, implying that the dissociation and diffusion processes are the rate-limiting steps for hydrogen electrochemical oxidation reaction. The R_2 of the LSCM–40SDC anode is markedly reduced as the SDC interlayer is introduced between the anode and YSZ electrolyte, indicating that the SDC interlayer plays an important role in promoting the dissociation and diffusion processes of H_2 oxidation reaction. The SDC interlayer is beneficial for several reasons. First, it exhibits mixed ionic and electronic conductivity in reducing environment due to the reduction of Ce^{4+} to Ce^{3+}, which expands the reaction zone beyond the TPB. Second, the ionic conductivity of SDC is higher than that of YSZ at intermediate temperature (600–800 °C), which improves the transport of oxygen ions from the electrolyte to the anode [20].

The SEM image of the cross-section of the LSCM–40SDC anode with the SDC interlayer is shown in Fig. 7. The YSZ electrolyte is dense and uniform. The LSCM–40SDC anode and SDC interlayer have suitable porosity. The thicknesses of the porous LSCM–40SDC anode and SDC interlayer are approximately 20 and 10 μm, respectively. The interfaces of the electrolyte–interlayer and interlayer–anode exhibit good adhesion. In addition, the anode with a high SDC content shows area contact between small particles, resulting in the lower contact resistance and better electrochemical performance of the LSCM–40SDC anode with the SDC interlayer.

The promotion of H_2 oxidation reaction by adding the SDC interlayer is also demonstrated by the polarization curves (Fig. 8). The anodic overpotential of LSCM–40SDC with the SDC interlayer is 0.035 V at a current density of 0.05 A cm^{-2} at 800 °C, which is 3.4 times lower than that of LSCM–40SDC without the SDC interlayer.

4. Conclusions

LSCM–SDC composite anodes were fabricated and investigated as anode materials for IT-SOFCs with YSZ electrolyte. The XRD patterns showed that the perovskite material LSCM and the cubic fluorite material SDC were synthesized by the solid state reaction method and that LSCM had good chemical compatibility with SDC at temperatures up to 1300 °C. The addition of SDC had no significant effect on the thermal expansion but decreased the conductivity of composite anodes. SDC played important roles in enhancing the electrochemical performance of LSCM. The polarization resistance and anodic overpotential (at a current density of 0.05 A cm^{-2}) in H_2 at 800 °C of the optimal anode, LSCM–40SDC, reduced by factors of 3.9 and 3.2, respectively, when compared with pure LSCM. Furthermore, the electrochemical performance of the composite anode was improved by introducing a thin SDC interlayer between the anode and YSZ electrolyte. The SDC interlayer mainly decreased the polarization resistance associated with low frequency, indicating that the SDC interlayer significantly promoted the dissociation and diffusion processes of H_2 oxidation reaction.

Acknowledgments

This work was supported by the Graduate Science and Technology Innovation Foundation of Jiangsu (CXZZ13_0419) and the Priority Academic Program Development of Jiangsu Higher Education Institutions (PAPD). We also acknowledge the support of Program for Changjiang Scholars and Innovative Research Team in University (PCSIRT), IRT1146.

References

[1] N.Q. Minh, J. Am. Ceram. Soc. 76 (1993) 563–588.
[2] S. Tao, J.T.S. Irvine, J. Electrochem. Soc. 151 (2004) A252–A259.
[3] C. Sun, U. Stimming, J. Power Sources 171 (2007) 247–260.
[4] D. Simwonis, F. Tietz, D. Stvöer, Solid State Ionics 132 (2000) 241–251.
[5] B.B. Patil, S.H. Pawar, J. Alloys Compd. 509 (2011) 3644–3650.
[6] Y. Matsuzaki, I. Yasuda, Solid State Ionics 132 (2000) 261–269.
[7] S. Park, J.M. Vohs, R.J. Gorte, Nature 404 (2000) 265–267.
[8] J.W. Fergus, Solid State Ionics 177 (2006) 1529–1541.
[9] J.B. Goodenough, Y.H. Huang, J. Power Sources 173 (2007) 1–10.
[10] J. Sfeir, P.A. Buffat, P. Möckli, N. Xanthopoulos, R. Vasquez, H.J. Mathieu, J. Van herle, K.R. Thampi, J. Catal. 202 (2001) 229–244.
[11] J. Sfeir, J. Power Sources 118 (2003) 276–285.
[12] S. Tao, J.T.S. Irvine, Nat. Mater. 2 (2003) 320–323.
[13] S.P. Jiang, X.J. Chen, S.H. Chan, J.T. Kwok, K.A. Khor, Solid State Ionics 177 (2006) 149–157.
[14] S.P. Jiang, X.J. Chen, S.H. Chan, J.T. Kwok, J. Electrochem. Soc. 153 (2006) A850–A856.
[15] X.J. Chen, Q.L. Liu, K.A. Khor, S.H. Chan, J. Power Sources 165 (2007) 34–40.
[16] M.K. Rath, B.H. Choi, K.T. Lee, J. Power Sources 213 (2012) 55–62.
[17] J.C. Ruiz-Morales, J. Canales-Vázquez, B. Ballesteros-Pérez, J. Peña-Martínez, D. Marrero-López, J.T.S. Irvine, P. Núñez, J. Eur. Ceram. Soc. 27 (2007) 4223–4227.
[18] S.P. Jiang, S.H. Chan, J. Mater. Sci. 39 (2004) 4405–4439.
[19] X.F. Ye, S.R. Wang, Z.R. Wang, Q. Hu, X.F. Sun, T.L. Wen, Z.Y. Wen, J. Power Sources 183 (2008) 512–517.
[20] E.P. Murray, T. Tsai, S.A. Barnett, Nature 400 (1999) 649–651.

[21] K. Eguchi, T. Setoguchi, T. Inoue, H. Arai, Solid State Ionics 52 (1992) 165–172.
[22] G.B. Balazs, R.S. Glass, Solid State Ionics 76 (1995) 155–162.
[23] Y. Zheng, S. He, L. Ge, M. Zhou, H. Chen, L. Guo, Int. J. Hydrogen Energy 36 (2011) 5128–5135.
[24] J.H. Yu, G.W. Park, S. Lee, S.K. Woo, J. Power Sources 163 (2007) 926–932.
[25] L. Deleebeeck, J.L. Fournier, V. Birss, Solid State Ionics 181 (2010) 1229–1237.
[26] B. He, L. Zhao, S. Song, T. Liu, F. Chen, C. Xia, J. Electrochem. Soc. 159 (2012) B619–B626.
[27] A. Babaei, L. Zhang, S.L. Tan, S.P. Jiang, Solid State Ionics 181 (2010) 1221–1228.
[28] X. Zhu, K. Sun, S. Le, N. Zhang, Q. Fu, X. Chen, Y. Yuan, Electrochim. Acta 54 (2008) 862–867.